

# Molecular BioSystems

Accepted Manuscript



This is an *Accepted Manuscript*, which has been through the Royal Society of Chemistry peer review process and has been accepted for publication.

*Accepted Manuscripts* are published online shortly after acceptance, before technical editing, formatting and proof reading. Using this free service, authors can make their results available to the community, in citable form, before we publish the edited article. We will replace this *Accepted Manuscript* with the edited and formatted *Advance Article* as soon as it is available.

You can find more information about *Accepted Manuscripts* in the [Information for Authors](#).

Please note that technical editing may introduce minor changes to the text and/or graphics, which may alter content. The journal's standard [Terms & Conditions](#) and the [Ethical guidelines](#) still apply. In no event shall the Royal Society of Chemistry be held responsible for any errors or omissions in this *Accepted Manuscript* or any consequences arising from the use of any information it contains.



[www.rsc.org/molecularbiosystems](http://www.rsc.org/molecularbiosystems)

# Antigenic Peptide Molecular Recognition by DRB1 - DQB1 Haplotype modulates Multiple Sclerosis Susceptibility

Amit Kumar<sup>1,2\*</sup>, Paola Melis<sup>1</sup>, Vito Genna<sup>1</sup>, Eleonora Cocco<sup>2</sup>, Maria Giovanna Marrosu<sup>2</sup>,  
and Enrico Pieroni<sup>1\*</sup>

<sup>1</sup> CRS4 Biomedicine, Science and Technology Park, Piscinamanna, Pula, Italy.

<sup>2</sup> Public Health and Clinical and Molecular Medicine, University of Cagliari, Italy.

\* Corresponding authors (akumar@crs4.it, ep@crs4.it).

**Abstract**

Multiple Sclerosis (MS) is an autoimmune disease of the central nervous system that has a notably high incidence in Sardinia. Our study focuses on two HLA class II haplotypes associated with the disease in Sardinia, the rare predisposing DRB1\*15:01-DQB1\*06:02 and the widespread protective DRB1\*16:01-DQB1\*05:02. This framework enabled the highlighting of HLA binding pocket specificity and peptide recognition mechanisms, by employing molecular dynamics simulations of the whole DRB1-DQB1 haplotype interacting with MBP- and EBV-derived peptides. We analyzed peptide-protein interaction networks and temporal evolution of the original complexes and after key amino acid mutations. The mutation G86V of the protective DRB1 allele exerted its effect mainly in presence of the EBV viral peptide, with local and long range outcomes. However, the V38A mutation of the protective DQB1 showed a long range effect only in the case of the MBP myelin peptide. Our findings demonstrate also a DRB1/DQB1 complementary molecular recognition of peptides. This mechanism could provide a robust synergistic action and a differential role of DRB1 and DQB1 role in tissues and in the time-steps towards autoimmunity. In addition, we demonstrate that negatively charged residues in pocket 4 and 9 play a role in MS susceptibility. Our findings are supported by recent experiments of a closely related MS animal model. Overall, our analysis confirms the role of DRB1-DQB1 haplotype in conferring disease predisposition and could provide a valuable aid in designing optimal therapeutic peptides for MS therapy.

**Keywords:** Multiple sclerosis; Molecular modeling; HLA antigen presentation; Molecular mimicry; DR-DQ cooperation.

## 1. Introduction

The main objective of the present study is to investigate the structural and dynamical aspects of peptide-binding characteristics of predisposing (DRB1\*15:01-DQB1\*06:02) and protective (DRB1\*16:01-DQB1\*05:02) haplotypes associated to Multiple Sclerosis (MS) in Sardinian population.<sup>1</sup>

MS is a chronic inflammatory disease, characterized by a major malfunction of the immune system and results in axon demyelination in the central nervous system.<sup>2</sup> Increasing evidence suggests that the disease is caused by the interaction of a predisposing genetic pattern and exposure to largely unknown triggering environmental factors.<sup>3</sup> This picture is shaped by the convergence of many low-weight factors. Early genetic studies identified the Human Leukocyte Antigen (HLA), also known as Major Histocompatibility Complex (MHC) system, in particular class II, as the main region linked to MS.<sup>4</sup> Increased certainty about this link was achieved through genome-wide association and candidate gene studies. This research also led to the discovery of new linked genes.<sup>5</sup> The analysis developed in these studies contain limitations that stem from: small genotype sample size, DNA linkage disequilibrium, small number of markers and neglect of post-translational and epigenetic effects. In order to expand on these results it is important to investigate the functional dynamics of the disease at a molecular level.<sup>6</sup>

Molecular mimicry has been proposed since many years as a relevant mechanism in the process leading to many autoimmune diseases, including MS,<sup>7</sup> which is the focus of our study. In this light, our aim is to investigate the presence of similar molecular interactions between specific myelin-derived and viral peptides, with respect to a given MHC

protein(molecular mimicry), because this can provide a molecular basis for the autoimmune response.<sup>8-11</sup>

Recently, a set of MS-resistant and permissive HLA DRB1-DQB1 haplotypes with respect to MS in Sardinian patients was identified.<sup>12</sup> We demonstrated that a polymorphism Gly/Val at DRB1 position 86 for a set of alleles (belonging to DR2 serotype) and the more conservative polymorphism Val/Ala at DQB1 38, characterized MS protective and predisposing haplotypes, respectively.<sup>12</sup> Unlike DRB1 86, to best of our knowledge, DQB1 site 38 has not yet been investigated in a complete and satisfactory way. In another work, we observed that eight susceptible DRB1 alleles in Sardinian population cluster in a few groups.<sup>1</sup> We had thus hypothesized that the functional mechanisms linking the HLA proteins to MS could vary in the different clusters. This observation is confirmed in the present work, and extended to include the phylogenetic classification of whole DRB1-DQB1 haplotypes (Fig. 1). This variability in the functional mechanisms partially explains the difficulties in finding a common factor that distinguishes between the contrasting allele roles in the disease's onset and progression.

Regarding MS immunogenic peptides, clinical research, animal models and immunological assays indicate that the most important auto antigens are derived from myelin proteins, which play different roles in distinct MS phases.<sup>11</sup> In the context of DR2 serotype group, the human immunodominant self-epitope is MBP 85-98 (Myelin Basic Protein).<sup>13</sup> For non-self antigens, we focused on Epstein Barr Virus (EBV), a candidate widely proposed as a potential environmental triggering agent.<sup>8, 14</sup> We are here referring specifically to a recent finding of an immunogenic EBV nuclear protein-derived peptide, EBNA1 400-413, in MS patients.<sup>15</sup>

Previously, we employed molecular dynamics simulations in a simplified and controlled framework<sup>16</sup> in order to understand the molecular mechanism underlying MS. We focused on two DRB1 alleles belonging to DR2 serotype group, i.e the predisposing DRB1\*15:01 and the protective DRB1\*16:01, and observed their interaction networks with myelin- and viral-derived peptides.<sup>16</sup> In the present study, we extend the work to the whole haplotypes and perform simulations of the following HLA proteins in complex with MBP- and EBNA1-derived peptides: (i) protective (DQB1\*06:02) and predisposing DQB1 (DQB1\*05:02), (ii) mutant of protective (DRB1\*16:01 G86V) and predisposing DRB1 (DRB1\*15:01 V86G), (iii) mutant of protective (DQB1\*05:02 V38A) and predisposing DQB1 (DQB1\*06:01 A38V).

For each peptide-MHC (pMHC) complex (Fig. 2), we have extensively analyzed the local flexibility and other dynamical features, including H-bond, aromatic stacking, binding free energy, which highlight the molecular basis of peptide-recognition in antigen presentation in the context of MS linked proteins. The analysis of pMHC binding cleft width fluctuations in time, in general, enables the identification of: i) allosteric changes and distinct protein conformations, particularly relevant for peptide loading, locking and release<sup>17</sup> ii) motifs for generic or specific peptide anchoring; iii) links between complex flexibility and disease susceptibility<sup>18, 19</sup> iv) role of peptide length and shift register in binding,<sup>20</sup> v) geometrical and physicochemical characteristics of the external surface available for TCR recognition and binding<sup>21</sup> vi) small synthetic ligands enhancing or reducing biological peptide binding.<sup>17</sup> On the other hand, H-bond interactions are known to contribute significantly to the stability of pMHC complexes,<sup>22</sup> and their impact on pMHC transport within the cell.<sup>23</sup> Finally, stacking interactions were shown to increase immunogenicity of the pMHC complex for class I.<sup>24</sup>

The connection between pMHC dynamical features, T cell binding affinities and triggering efficacy for a given pMHC and T cell activation is complex. Nevertheless, a common thread joining some of these aspects has been recently proposed,<sup>18, 25, 26</sup> based on enhanced peptide loading capabilities,<sup>27-30</sup> reciprocal conformational plasticity of both TCR and pMHC,<sup>25, 31-33</sup> conformational adjustment upon TCR binding.<sup>34, 35</sup> We limit ourselves to observe here the ability of peptides to bind successfully to MHC proteins is the prerequisite for an efficient recognition of pMHC complexes by T-cells. This is a fundamental step for the initiation of an immune response.<sup>2</sup> In general, antigenic peptides have been broadly classified as binders ( $IC_{50} \leq 1000$  nM) and as non-binders ( $IC_{50} \geq 1000$  nM) to MHC proteins in binding assays experiments.<sup>36</sup>

## 2. Results

### 2.1 Binding cleft width probability distributions

To study pMHC flexibility, and following a recent approach,<sup>37</sup> we divided the MHC binding groove into four compartments (Fig. 3) corresponding respectively to the influence region of the pockets 1, 4, 7 and 9.<sup>16</sup> Next, we analyzed the binding cleft width probability distribution in each region during extended simulations of wild types and mutated DQB1 and DRB1 complexes. Note that mutation site 86 in DRB1 is positioned in region D1/pocket 1 (Fig. 3B), while mutation site 38 in DQB1 is positioned in region D4/pocket 9 (Fig. 3A). We present in the following sections the results for each allele, according to this general scheme: first wild type allele with both peptides (MBP, EBNA1), then wild type allele free and thereafter mutant allele bound to both peptides.

#### ***Protective allele DQB1\*05:02***

For the protective allele DQB1\*05:02 in complex to MBP and EBNA1 peptides, we observe an interesting feature of width profile in region D1, with both complexes sharing a common local curve peaked at  $\sim 13$  Å (Fig. 4A), and the MBP complex alone showing a narrower and less populated configuration centered at  $\sim 9$  Å. For region D2, we note a similar profile across the whole width range for both peptide complexes (supplementary material, Fig. S1). In region D3, EBNA1 complex displays a slightly wider distribution profile with smaller peak value ( $\sim 1$  Å) with respect to MBP complex (supplementary material, Fig. S1). In region D4, MBP complex displays a relatively narrow and tall distance distribution profile with peak values right shifted by  $\sim 1.5$  Å with respect to the EBNA1 complex (Fig. 4B). Next, for the unbound protective allele case, we noted that region D1 is very flexible (width fluctuation in the range 9-21 Å), while the width distribution for D2 and D3 regions is left shifted with respect to the peptide bound cases (supplementary material, Fig. S1). In region D4, the unbound protective allele displayed a nearly identical distribution profile as the EBNA1 complex (Fig. 4B), and a moderate difference in height. The effect of mutation V38A (which belongs to region D4, Fig. 3A) on the protective allele produced a pronounced long-range effect in region D1 (inset of Fig. 4A), particularly for the MBP complex. More precisely, the mutated allele in complex with the MBP exhibited a unique distribution peaked at an intermediate distance of  $\sim 10.5$  Å, with a width of  $\sim 2$  Å, resulting in a less flexible configuration than the wild type (inset of Fig. 4A). There was also an increase in local cleft flexibility in the region D4, upon mutation of the protective allele in complex with MBP (inset of Fig. 4B).

***Predisposing allele DQB1\*06:02***

For the predisposing allele DQB1\*06:02, we observe a similar width distribution profile in region D1 for both bound and unbound MHC cases (supplementary material, Fig. S2). However, the allele bound to EBNA1 peptide displayed a distance profile left shifted in D2 (Fig. 4C), D3 (Fig. 4D) and D4 regions (supplementary material, Fig. S2), with respect to MBP bound case. Interestingly, there is a bimodal distribution of the EBNA1 complex in D2 (peaking at  $\sim 13$  Å and  $\sim 15$  Å, inset Fig. 4C), mirrored by the MBP complex in D3 (peaking at  $\sim 18.5$  Å and  $\sim 21$  Å, inset Fig. 4D). For unbound predisposing DQB1 allele, there is a perfect profile overlap with the EBNA1 bound case in region D4 (supplementary material, Fig. S2). The effect of mutation A38V (located in region D4) on predisposing DQB1 allele produced a strikingly different width distribution profile in region D2 and D3, with respect to wild type counterparts, for both peptide complexes (Fig. 4C, Fig. 4D). A detailed analysis indicated that:

-upon the mutation A38V of MBP complex, the distance profile distribution in region D2 is left shifted and the curve in region D3 becomes narrower and left shifted (Fig. 4C, inset Fig. 4D);

-upon the mutation A38V of EBNA1 complex the distance profile distribution in regions D2 and D3 becomes wider and more flexible (inset Fig. 4C and Fig. 4D);

-region D4 in the mutated A38V predisposing allele, for both peptides complexes, displayed a more rigid distance distribution profile compared to respective wild types (supplementary material, Fig. S3), which is opposite to the effect of mutation V38A on the protective allele.

#### ***Protective allele DRB1\*16:01***

For the protective DRB1\*16:01 allele, the mutation G86V exerts its influence on binding cleft width distribution profile mainly locally and in a more pronounced manner for EBNA1

complex (Fig. 5A, 5B). No relevant differences were noted upon mutation of protective DRB1 allele for MBP bound case, with the exception of the D1 region, where the distance profile is shifted towards right (Fig. 5A). In particular, for EBNA1 complex, the mutation destroys the trimodal pattern observed in the regions D1 (Fig. 5A) and D2 (Fig. 5B) for wild type case, and replaces it with a single bell profile centered at  $\sim 12.5$  Å and with a width of  $\sim 2$  Å in both regions. The cleft distance profile in region D3 (inset Fig. 5A) and D4 (inset Fig. 5B) is shifted to right upon G86V mutation.

### ***Predisposing allele DRB1\*15:01***

For the predisposing DRB1\*15:01 allele bound to MBP peptide, mutation V86G introduces a higher flexibility in region D1 (Fig. 5C). The mutation V86G produces significant changes in binding cleft width profile for the EBNA1 complex with respect to the wild type case. In particular, in region D1 the characteristic bimodal distribution of the wild type case (Fig. 5C) gets destroyed upon V86G mutation and a unimodal distribution centered at  $\sim 10.5$  Å is observed. Upon the same mutation for EBNA1 complex, the distance distribution curve gets shifted towards right for region D2 (Fig. 5D) and for regions D3 (inset Fig. 5C) and towards left for D4 (inset Fig. 5D).

## **2.2 Hydrogen bonds**

Here, we evaluated H-bond interactions for all pMHC complexes under investigation with a persistence of at least 20% of the 100 ns MD simulation time, to probe their relevance for pMHC affinity and peptide immunogenicity in the context of MS disease.

### ***Peptide-DQB1 interaction***

Three common binding site residues (W61, H81 and N82) across both DQB1 alleles (DQB1\*06:02, DQB1\*05:02) are involved in H-bond interactions with different MBP

residues (Fig. 6, 7). We also found allele-characteristic binding site residues (supplementary material, Table S1) participating in H-bond interaction with MBP: R77 for DQB1\*05:02 (Fig. 6A, 7A), Y30 and E74 for DQB1\*06:02 (Fig. 6B, 7B). With regard to the EBNA1 complex, durable H-bonds were formed in both DQB1 alleles as a result of the interaction of two common binding site residues, W61 and N82 (Fig. 6C-D, 8). Additional allele-characteristic binding site residues are: H30 for DQB1\*05:02 (Fig. 6C, 8A, Table S1), and D57 and E74 for DQB1\*06:02 allele (Fig. 6D, 8B). Upon mutation V38A of DQB1\*05:02 in the complex with both MBP (Fig. 7A) and EBNA1 peptides (Fig. 8A), the majority of the interacting pairs is conserved, with two relevant exceptions in the MBP peptide complex. In detail: the H-bond interaction involving residue R77 (Fig. 7A) was completely absent, while there were very transient interactions involving residue Y37 (Fig. 7A). On the other hand, for mutant A38V DQB1\*06:02 in complex with MBP (Fig. 7B), a characteristic H-bond interaction involving residue D57 was observed, which was transient for the wild type allele. Finally, the mutant A38V DQB1\*06:02 in complex with EBNA1, compared to its wild type counterpart, generated an additional H-bond interacting pair for residue N82 and no H-bond interacting pair for residue E74 (Fig. 8B) was noted.

#### ***Peptide-DRB1 interaction***

For MBP bound to the mutant V86G DRB1\*15:01 (Fig. 9A) or mutant G86V DRB1\*16:01 (Fig. 9B), compared to their respective wild type counterparts (Fig. 9), we noted the absence of durable H-bond interactions with residues 13 and 70, and the presence of conserved interactions with residues 81 and 82 (Fig. 9). Interestingly, we also found a particular H-bond interaction between MBP peptide and binding site residue D57 (pocket 9), which is present only in the mutant G86V DRB1\*16:01 (Fig. 9B). For the EBNA1 complex, upon mutation

V86G of predisposing DRB1\*15:01, three important and conserved interactions involving residues R13, N82 and E87 were observed (Fig. 10A). The mutation G86V of protective DRB1\*16:01, bound to EBNA1 peptide, produced a completely new interaction network (Fig. 10B). As a whole, the total number of H-bond interactions between the mutant alleles and both the peptides is reduced with respect to their wild type counterparts (Fig. 9, 10).

### 2.3 Aromatic Stacking Interactions

The presence of aromatic stacking interaction has been recognized as an important component in the structure and function of proteins.<sup>38, 39</sup> Here, we evaluated persistent aromatic-aromatic stacking interactions (see Material and Methods) for all the pMHC complexes under investigation (Table 1). For the protective allele DQB1\*05:02 in complex with MBP peptide, we recorded an additional stacking interaction with a residue from both chains ( $\alpha$ R76 and  $\beta$ Y60), with respect to the EBNA1 complex. Contrastingly, for the predisposing DQB1\*06:02, fewer stacking interactions were observed involving both  $\alpha$ 1- and  $\beta$ 1-chain binding site residues for the MBP complex with respect to the EBNA1 complex. Compared to wild type simulation, the mutation of protective DQB1-MBP complex introduced a new interaction with a  $\beta$ 1-chain residue R77. Furthermore, only one stacking interaction  $\alpha$ Y22 was observed for mutant DQB1\*05:02 allele in complex with EBNA1 peptide. With respect to wild type simulations, there was a new stacking interaction involving  $\beta$ F11 residue upon mutation A38V of predisposing DQB1-MBP complex, while for the EBNA1 case the loss of the interaction with  $\beta$ H81 residue was evident. For MBP-DRB1 complexes (Table 1B), there was a loss of stacking interaction involving  $\beta$ 1-chain residue H81 upon mutation of DRB1\*15:01, while after mutation of DRB1\*16:01 we observed an increase in the total number of stacking interactions. Finally, it is noteworthy that upon the

mutation of DRB1 predisposing allele bound to EBNA1 peptide, emerged a new stacking interaction network involving mainly  $\alpha$ 1-chain residues (Table 1B).

#### 2.4 Binding energies

The approach we adopted was to first calculate the binding energies for all the pMHC complexes and then to converted them to  $IC_{50}$  values (see Material and Methods). Concerning wild type simulations (Table 2), protective allele DQB1\*05:02 produced a slightly more favorable binding when bound to MBP with respect to EBNA1 (difference of  $\sim 1.5$  kcal/mol). Predisposing allele DQB1\*06:02, on the other hand, displayed a much more favorable binding to EBNA1 with respect to MBP peptide (difference of  $\sim 3.4$  kcal/mol). The  $IC_{50}$  ratio of the EBNA1 and MBP complexes allowed for an immediate comparison of these results (Table 2). For DQB1 predisposing allele a very low  $IC_{50}$  ratio,  $4.6 \times 10^{-5}$ , was observed. This low ratio was suggestive of a very strong binding affinity of EBNA1 peptide for MHC compared to that of MBP peptide. In contrast, a ratio of 11 was obtained for DQB1 protective allele. For the complexes formed by the predisposing DQB1 allele upon A38V mutation, a more favorable binding free energy to both peptides, with respect to the wild type counterparts, was recorded (Table 3). On the other hand, quite similar binding energy values (within a difference of  $\sim 1$  kcal/mol) with respect to wild type simulations for both peptide complexes (Table 3), was observed upon mutation V38A of DQB1\*05:02.

For mutation V86G of predisposing DRB1 allele, with respect to its wild type counterpart, we noted a very similar binding energy when the mutant allele was bound to MBP peptide, while a more favorable energy (difference of  $\sim 2.4$  kcal/mol) was obtained for EBNA1 peptide (Table 3). Mutation G86V of protective DRB1 allele, however, resulted in very similar

binding free energies with respect to the wild type simulations, for both peptide complexes (difference of ~1 kcal/mol, Table 3).

### 3. Discussion

#### 3.1 Antigenic peptide recognition specificity and DRB1/DQB1 complementarity

As expected, we documented a higher global flexibility (higher RMSD value) for the free DQB1 alleles with respect to the bound peptide cases (Fig. 4), with the free protective DQB1 allele being more flexible than the free predisposing one (supplementary material, Table S2, Fig. S5). We found a peculiar ability of the predisposing DQB1 allele (Fig. 4D, Table 2) to discriminate the MBP- and EBNA1- peptides (see points 1 and 2 in the paragraph below). This behavior recalls what we observed for the DRB1 alleles in our previous work,<sup>16</sup> but it is characterized by a reverse signature, with the predisposing DQB1 allele behaving as the protective DRB1 one, thus suggesting a sort of complementarity of the DRB1 and DQB1 alleles in peptide molecular recognition. In Table 2, we report the binding energies obtained for the wild type pMHC systems investigated here. The EBNA1 to MBP IC<sub>50</sub> ratios (see 6<sup>th</sup> column in Table 2) lie within the range measured in experimental assays for DRB1\*15:01 binding to other non-self peptides derived from Herpes Virus 1, Hepatitis B Virus, Hepatitis C Virus and Human Immunodeficiency Virus (IEDB accession date October 21, 2013, Query: MHC binding, MHC restriction DRB1\*15:01).<sup>40</sup> The following points emerge comparing binding energies of the pMHC complexes (Table 2):

(1) The protective DRB1-DQB1 haplotype provides self and non-self peptide discrimination in two ways: DRB1 peptide binding allows a high level of discrimination between MBP and

EBNA1 derived peptides (difference of 5.3 kcal/mol, last column of Table 2), while DQB1 binding complements this feature with an intermediate discrimination ability (1.5 kcal/mol).

(2) The predisposing DRB1-DQB1 haplotype peptide discrimination ability is at a low level for the DRB1 allele (difference of 0.7 kcal/mol, last column of Table 2) and at an intermediate-to-high level for DQB1 (-3.4 kcal/mol).

(3) Affinity of both DRB1 and DQB1 for the MBP derived peptide is higher for the protective haplotype (0.8 and 4.4 kcal/mol, respectively last two rows in Table 2), while the opposite holds for the EBNA1 derived peptide (-3.8, -0.5 kcal/mol).

We interpret the first point as follows: the antigen presenting cell (APC) bearing the protective haplotype DRB1\*16:01-DQB1\*05:02 is able to present stable and presumably long-lived MBP-MHC complexes via both DRB1 and DQB1, and intermediate-lifetime EBNA1-MHC complex via only DQB1. Regarding the second point, the predisposing haplotype DRB1\*15:01-DQB1\*06:02 has in part lost “normal” discrimination ability, and in part shows inverted peptide roles in the discrimination process. Taken together, the first two points suggest MS predisposition may be linked to losing the ability to discriminate MBP- and EBNA1-derived peptides (functional mimicry) of both DRB1 and DQB1 alleles, and also to presence of a kind of DRB1/DQB1 complementarity. In synthesis, in the case of the two peptides investigated here, the DRB1 and DQB1 alleles seem to complement each other, and integrate their actions to make the whole molecular mimicry mechanism effective, wherein the predisposing DRB1-DQB1 haplotype exhibits a smaller peptide discrimination ability, and a higher affinity for EBNA1 with respect to MBP, than the protective one.

Recently a similar mechanism has been proposed,<sup>41</sup> in which the same TCR recognizes the same peptide in the context of different co-expressed HLA molecules, which is promiscuous

restriction. In particular, for the first time, the authors experimentally proved promiscuous restriction in action for DR and DQ co-expressed in a haplotype that is associated with MS.<sup>41</sup> The authors in this study hypothesized that this mechanism evolved to provide an advantage during infections – higher T cell activation efficiency due to a higher level of antigen presentation and recognition. But the higher activation could also be responsible for autoimmune responses in MS, increasing the risk of cross-reactivity. Other recent immunological findings are related to the result of the present work, although dealing with different peptides. There is some evidence from MS animal models (transgenic mice with HLA genetic background) in the context of PLP<sup>42</sup> and MOBP<sup>43</sup> MS susceptibility epitopes, that DQB1\*06:02 has a role in disease induction, independent from DRB1\*15:01.<sup>44</sup> In particular, DRB1\*15:01 and DQB1\*06:02 were found to differentially activate T lymphocytes, leading to strikingly different cytokine profiles. These were biased respectively toward Th2 and Th1/Th17 phenotypes, which are known to possess different impact on inflammatory processes. Although further detailed investigation with these specific peptides is required, the distinct roles of predisposing DRB1 and DQB1 alleles in interacting with the same peptide is also observed in our simulations.

### 3.2 In Silico mutations

In this section, we discuss the impact of single residue virtual mutations on the binding groove dynamics of DQB1 and DRB1 pMHC complexes. Mutation V38A in the protective DQB1 allele inside the complex with MBP peptide, induces a long-range effect (Fig. 4A, 4B), which is indicative of a cooperative interaction<sup>30</sup> between the region where the residue has been mutated (region D4, Fig. 4B) and the region in which the largest effect is observed (region D1, Fig. 4A). However, upon the specular A38V mutation of DQB1 predisposing

allele for both MBP and EBNA1 complexes, a cooperative interaction effect between the D2, D3 and D4 regions (inset Fig. 4C-D) is observed. Alteration in dynamics of region D4 (mutation site), for both mutants V38A (inset Fig. 4B) and A38V (supplementary material, Fig. S3) of DQ protein-peptide complexes is due to variation in amino acid size upon mutation.

Mutation G86V in the EBNA1-protective DRB1 complex has a global effect on the dynamics of the peptide binding groove (inset Fig. 5A-B). In detail, new H-bond interactions (Fig. 10B) between DRB1 residues and EBNA1 residues result in narrow D1 and D2 regions, while loss of H-bond interactions produces wider regions D3 and D4. On the other hand, mutation V86G of predisposing DRB1 allele alters predominantly the flexibility in region D1 for both pMHC complexes, which is due to steric effects (Fig. 5C). Moreover, the presence of durable H-bond interactions, H81-R403 and R13-P408 (Fig. 10A), produces a more rigid and narrower D1 region (Fig. 5C) for the EBNA1 complex. In contrast, a flexible D1 region results for MBP complex due to transient H-bond interactions (Fig. 9A). Overall, we found mutation to exert a stabilizing effect for the predisposing DRB1\*15:01 bound to EBNA1, and for the predisposing DQB1\*06:02 complexed to MBP (Table 3).

### 3.3 *pMHC interactions*

We examined the pattern of interactions, including H-bond, hydrophobic and aromatic stacking, between the DQB1 binding site and peptide residues (DRB1 allele was extensively studied in our previous work<sup>16</sup>). Note that DQB1 polymorphisms at residue positions 57, 74, and 77 (Fig. 6, supplementary material Table S1) are strikingly reflected in the HLA protein H-bond interactions with MBP- (Fig. 6A-B, Fig. 7) and the EBNA1-derived (Fig. 6C-D, Fig. 8) peptides. The role of these DQB1 polymorphic residues in autoimmune diseases

(particularly type 1 diabetes and narcolepsy), with specific recognition capabilities of antigenic fragments, has been postulated to be relevant for T-cell activation.<sup>45</sup> In particular, we observe H-bonds with D57 (pocket 9) and E74 (pocket 4, Fig. 6B, 6D) to characterize the DQB1 predisposing allele, while polar amino acid serine is present in the protective allele in these same positions (supplementary material, Table S1). H-bond interaction involving residue Arg 77 (Fig. 6A) characterizes the DQB1 protective allele when bound to MBP-derived peptide. Our findings thus suggest that the negative charged environment of pockets 4 and 9 are relevant for conferring MS predisposition to the DQB1 allele. Similarly, site 77 (supplementary material, Table S1) appears to be important in conferring protective DQB1 allele to distinguish between the two peptides analyzed here.

### **3.4 Final remarks**

In conclusion, we highlighted the molecular basis of peptide recognition based on the MD simulations of a relatively simple model, composed of two HLA haplotypes (predisposing and protective) and two peptides (MBP- and EBNA1-derived), relevant for MS in Sardinian population. Their punctual interpretation within the wider context of MS disease will require further investigation to integrate other pMHC models, other experimental findings and the entire complex of pMHC and TCR in selected cases. The observed DRB1/DQB1 complementarity in antigenic peptide recognition, and the resulting DRB1/DQB1 differential role in tissues, will also provide a valuable aid in designing optimal therapeutical peptides<sup>46</sup> for MS targeted therapies.

## **4. Material and Methods**

### **4.1 Model preparation**

The starting structure for the protective allele DQB1 \*05:02 in complex with MBP 85-98 peptide (supplementary material, Table S1) was derived from the X-ray structure (PDB access code: 3PL6), that also contained the TCR component. For predisposing allele DQB1\*06:02, we chose the available X-ray structure (PDB access code: 1UVQ), in complex with hypocretin peptide. The model structure of the complex DQB1\*05:02 and EBNA1 400-413 (supplementary material, Table S1) was obtained by homology modeling using the available 3PL6 template, through the web-server MODPROPEP.<sup>47</sup> We used the same web tool to model the structures of DQB1\*06:02-MBP and DQB1\*06:02-EBNA1 complexes using the available 1UVQ template. The initial structures for the HLA-DRB1 peptide complexes were taken from our recent work.<sup>16</sup> The single residue mutations (positions DQB1 38 and DRB1 86) of the alleles in complex with both peptides were performed using the module Mutator available in the VMD software.<sup>48</sup> Missing hydrogen atoms in the final models were added using VMD software and the systems were subsequently placed in a rectangular water box where counter-ions were added for neutralization (Fig. 2).

#### 4.2 Simulations

Initially, we performed energy minimization for each individual peptide-HLA complex system, followed by a gradual heating of the system up to 310 K in steps of 30 K, constraining positions of C-alpha atoms to 50 kcal/(mol Å<sup>2</sup>).<sup>16, 49</sup> The constraints on the C-alpha atoms were then relaxed in steps of 10 kcal/(mol Å<sup>2</sup>) within a 0.3 ns simulation time. Each molecular system was then subjected to an equilibration run of 3 ns, followed by a production run of 100 ns full simulation time, performed in the statistical ensemble with constant pressure, temperature and number of atoms and using periodic boundary conditions.

We adopted Charmm27<sup>50</sup> force-field parameters for the protein and ions and TIP3P<sup>51</sup> parameters for water molecules. The initial dimension of the edges of simulation box for the DQB1 complexes is {80, 96, 74} Å, while for DRB1 systems it is {77, 75, 96} Å, for a total number of ~50,000 atoms in each system. All bonds involving Hydrogen atoms were constrained using SHAKE,<sup>52</sup> which allows an integration time step of 2 fs. The long-range electrostatic interactions were evaluated using particle mesh Ewald with a {96 96 96} Å grid dimension. We used a 10 Å cut-off radius for both Van der Waals and electrostatic interactions.<sup>53</sup> All simulations were performed using the NAMD<sup>54</sup> software package on a 64 cores processor cluster.

### 4.3 Analysis

The stability of the MHC-peptide complex was checked by evaluating the root mean square deviation (RMSD, supplementary material Table S2, Fig. S5) and root mean square fluctuations (supplementary material, Fig. S6-S9) of the C-alpha atoms for the selected binding site residues. As the peptide binding groove is ~40 Å long, we divided it into four compartments<sup>16, 37</sup> (D1, D2, D3 and D4) as shown in Fig. 3. The center of mass distance variation of heavy atoms between the selected residues of  $\alpha$  and  $\beta$  chains (see Fig. 3 for the selection) was calculated on the MD trajectory, for each of the molecular systems investigated in our study. The peptide binding groove for both DQB1 and DRB1 alleles was divided into four regions (Fig. 3), as previously described.<sup>16, 37</sup> The center of mass distance variation of the heavy atoms for the residues included in the four regions was then calculated during 100 ns MD simulation.

H-bond interactions between the peptide and binding site residues were calculated using the Donor-Acceptor cutoff distance of 3.1 Å and cutoff angle of 130°, while the aromatic stacking interactions were calculated using EUCB software<sup>55</sup> with 30° cutoff for dihedral angle between the planar/ring side chains, centroid distance cutoff between side chains of 5.0 Å, and a minimum duration of 20% of simulation time. The binding energy for the peptide-MHC complexes was evaluated using solvated interaction energy (SIE) method.<sup>56</sup> In SIE method, the peptide-MHC binding energy ( $\Delta G_{\text{bind}}$ ) in aqueous solution is approximated by (i) an interaction energy contribution ( $E_{\text{inter}}$ ) and (ii) a desolvation free energy contribution ( $\Delta G_{\text{desolv}}$ ), which resembles the formalism used in MM-PBSA.<sup>57</sup> Even though entropy is not explicitly included, calibration of obtained SIE free energy is done by an empirically determined parameter, obtained by fitting a training set of 99 protein-ligand complexes, thus allowing a crude but effective treatment of entropy-enthalpy compensation. Additional MD simulations of pMHC complexes was performed using Amber 99 force-field parameters,<sup>58</sup> a prerequisite for using SIETRAJ software package.<sup>59</sup> The binding energy was then calculated at time step of 20 ps for a total simulation time of 30 ns. From the obtained binding energy values we then obtained their respective  $IC_{50}$  value (equivalent to the association constant), which corresponds to concentration of peptide required to bind 50% of MHC protein, using the standard relation  $\Delta G \approx k_B T \ln(IC_{50})$ .<sup>60</sup>

### **Acknowledgment**

PM and VG thank CRS4 for hosting their internships. Special thanks to S.A.R. Coleridge, G.J. Brelstaff and A.L. Scheinine.

### Supplementary Material

Supporting information can be found in the file “Supplementary\_material\_Kumar\_et.al.pdf“, which has been attached separately.

### References

1. E. Cocco, R. Murru, G. Costa, A. Kumar, E. Pieroni, C. Melis, L. Barberini, C. Sardu, L. Loreface, G. Fenu, et al., *PLoS One*, 2013, **8**, e59790.
2. J. R. Oksenberg, S. E. Baranzini, S. Sawcer and S. L. Hauser, *Nat Rev Genet*, 2008, **9**, 516-526.
3. S. E. Baranzini, *Curr Opin Genet Dev*, 2011, **21**, 317-324.
4. S. V. Ramagopalan, J. C. Knight and G. C. Ebers, *Curr Opin Neurol*, 2009, **22**, 219-225.
5. C. International Multiple Sclerosis Genetics, C. Wellcome Trust Case Control, S. Sawcer, G. Hellenthal, M. Pirinen, C. C. Spencer, N. A. Patsopoulos, L. Moutsianas, A. Dilthey, Z. Su, et al., *Nature*, 2011, **476**, 214-219.
6. L. Fugger, M. A. Friese and J. I. Bell, *Nat Rev Immunol*, 2009, **9**, 408-417.
7. E. M. Chastain and S. D. Miller, *Immunol Rev*, 2012, **245**, 227-238.
8. K. Kakalacheva and J. D. Lunemann, *FEBS Lett*, 2011, **585**, 3724-3729.
9. C. Münz, J. D. Lünemann, M. T. Getts and S. D. Miller, *Nat Rev Immunol*, 2009, **9**, 246-258.
10. S. Aggarwal, L. Yurlova and M. Simons, *Trends Cell Biol*, 2011, **21**, 585-593.

11. R. O. Jorge, E. B. Sergio and L. H. Stephen, in *Multiple Sclerosis Therapeutics*, ed. R. O. Jorge, Informa Healthcare, 2007, pp. 23-44.
12. E. Cocco, C. Sardu, E. Pieroni, M. Valentini, R. Murru, G. Costa, S. Tranquilli, J. Frau, G. Coghe, N. Carboni, et al., *PLoS One*, 2012, **7**, e33972.
13. G. Harauz, V. Ladizhansky and J. M. Boggs, *Biochemistry*, 2009, **48**, 8094-8104.
14. E. Sundqvist, P. Sundstrom, M. Linden, A. K. Hedstrom, F. Aloisi, J. Hillert, I. Kockum, L. Alfredsson and T. Olsson, *Genes Immun*, 2012, **13**, 14-20.
15. R. Mechelli, J. Anderson, D. Vittori, G. Coarelli, V. Annibali, S. Cannoni, F. Aloisi, M. Salvetti, J. A. James and G. Ristori, *Mult Scler*, 2011, **17**, 1290-1294.
16. A. Kumar, E. Cocco, L. Atzori, M. G. Marrosu and E. Pieroni, *PLoS One*, 2013, **8**, e59711.
17. H. Zaheer ul and W. Khan, *J Comput Aided Mol Des*, 2011, **25**, 81-101.
18. B. Knapp, U. Omasits, W. Schreiner and M. M. Epstein, *PLoS One*, 2010, **5**, e11653.
19. L. J. Carreno, P. A. Gonzalez and A. M. Kalergis, *Immunobiology*, 2006, **211**, 47-64.
20. S. Gunther, A. Schlundt, J. Sticht, Y. Roske, U. Heinemann, K. H. Wiesmuller, G. Jung, K. Falk, O. Rotzschke and C. Freund, *Proc Natl Acad Sci U S A*, 2010, **107**, 22219-22224.
21. K. W. Wucherpfennig, E. Gagnon, M. J. Call, E. S. Huseby and M. E. Call, *Cold Spring Harb Perspect Biol*, 2010, **2**, a005140.
22. B. J. McFarland, C. Beeson and A. J. Sant, *J Immunol*, 1999, **163**, 3567-3571.
23. A. V. Chervonsky, L. Gordon and A. J. Sant, *Int Immunol*, 1994, **6**, 973-982.
24. T. J. Kirksey, R. R. Pogue-Caley, J. A. Frelinger and E. J. Collins, *J Biol Chem*, 1999, **274**, 37259-37264.

25. J. J. Adams, S. Narayanan, B. Liu, M. E. Birnbaum, A. C. Kruse, N. A. Bowerman, W. Chen, A. M. Levin, J. M. Connolly, C. Zhu, et al., *Immunity*, 2011, **35**, 681-693.
26. A. Ferrante, *Immunol Res*, 2012, **56**, 85-95.
27. S. Sadegh-Nasseri, S. Natarajan, C. L. Chou, I. Z. Hartman, K. Narayan and A. Kim, *Immunol Res*, 2010, **47**, 56-64.
28. B. Rupp, S. Gunther, T. Makhmoor, A. Schlundt, K. Dickhaut, S. Gupta, I. Choudhary, K. H. Wiesmuller, G. Jung, C. Freund, et al., *PLoS One*, 2011, **6**, e18662.
29. M. J. Call, *Mol Immunol*, 2011, **48**, 1735-1743.
30. A. Ferrante and J. Gorski, *J Mol Biol*, 2012, **417**, 454-467.
31. M. Harkiolaki, S. L. Holmes, P. Svendsen, J. W. Gregersen, L. T. Jensen, R. McMahon, M. A. Friese, G. van Boxel, R. Etzensperger, J. S. Tzartos, et al., *Immunity*, 2009, **30**, 348-357.
32. D. R. Scott, O. Y. Borbulevych, K. H. Piepenbrink, S. A. Corcelli and B. M. Baker, *J Mol Biol*, 2011, **414**, 385-400.
33. C. J. Holland, P. J. Rizkallah, S. Vollers, J. M. Calvo-Calle, F. Madura, A. Fuller, A. K. Sewell, L. J. Stern, A. Godkin and D. K. Cole, *Sci Rep*, 2012, **2**, 629.
34. P. Csermely, R. Palotai and R. Nussinov, *Trends Biochem Sci*, 2010, **35**, 539-546.
35. C. F. Reboul, G. R. Meyer, B. T. Porebski, N. A. Borg and A. M. Buckle, *PLoS Comput Biol*, 2012, **8**, e1002404.
36. P. Wang, J. Sidney, C. Dow, B. Mothe, A. Sette and B. Peters, *PLoS Comput Biol*, 2008, **4**, e1000048.
37. R. Yaneva, S. Springer and M. Zacharias, *Biopolymers*, 2009, **91**, 14-27.
38. K. E. Riley and P. Hobza, *Acc Chem Res*, 2013, **46**, 927-936.

39. T. Balaraju, A. Kumar, C. Bal, D. Chattopadhyay, N. Jena, N. C. Bal and A. Sharon, *Struct Chem*, 2013, **24**, 1499-1512.
40. J. Ponomarenko, N. Papangelopoulos, D. M. Zajonc, B. Peters, A. Sette and P. E. Bourne, *Nucleic Acids Res*, 2010, **39**, D1164-D1170.
41. M. Sospedra, P. A. Muraro, I. Stefanova, Y. Zhao, K. Chung, Y. Li, M. Giulianotti, R. Simon, R. Mariuzza, C. Pinilla, et al., *J Immunol*, 2006, **176**, 1951-1961.
42. N. Kaushansky, D. M. Altmann, C. S. David, H. Lassmann and A. Ben-Nun, *J Neuroinflammation*, 2012, **9**, 29.
43. N. Kaushansky, M. Eisenstein, R. Zilkha-Falb and A. Ben-Nun, *Autoimmun Rev*, 2010, **9**, 233-236.
44. N. Kaushansky, D. M. Altmann, S. Ascough, C. S. David, H. Lassmann and A. Ben-Nun, *J Immunol*, 2009, **183**, 3531-3541.
45. M. G. Rudolph, R. L. Stanfield and I. A. Wilson, *Ann Rev Immunol*, 2006, **24**, 419-466.
46. L. Steinman, *Neurotherapeutics*, 2007, **4**, 661-665.
47. N. Kumar and D. Mohanty, *Nucleic Acids Res*, 2007, **35**, W549-555.
48. W. Humphrey, A. Dalke and K. Schulten, *J Mol Graph*, 1996, **14**, 33-38, 27-38.
49. A. Kumar, E. Hajjar, P. Ruggerone and M. Ceccarelli, *J Phys Condens Matter*, 2010, **22**, 454125.
50. A. D. MacKerell, Jr., N. Banavali and N. Foloppe, *Biopolymers*, 2000, **56**, 257-265.
51. W. L. Jorgensen, J. Chandrasekhar, J. D. Madura, R. W. Impey and M. L. Klein, *J Chem Phys*, 1983, **79**, 926.
52. J.-P. Ryckaert, G. Ciccotti and H. J. C. Berendsen, *J Comput Phys*, 1977, **23**, 327-341.

53. U. Essmann, L. Perera, M. L. Berkowitz, T. Darden, H. Lee and L. G. Pedersen, *J Chem Phys*, 1995, **103**, 8577.
54. J. C. Phillips, R. Braun, W. Wang, J. Gumbart, E. Tajkhorshid, E. Villa, C. Chipot, R. D. Skeel, L. Kale and K. Schulten, *J Comput Chem*, 2005, **26**, 1781-1802.
55. I. G. Tsoulos and A. Stavrakoudis, *Computer Physics Communications*, 2011, **182**, 834-841.
56. M. Naim, S. Bhat, K. N. Rankin, S. Dennis, S. F. Chowdhury, I. Siddiqi, P. Drabik, T. Sulea, C. I. Bayly, A. Jakalian, et al., *J Chem Inf Model*, 2007, **47**, 122-133.
57. J. Wang, P. Morin, W. Wang and P. A. Kollman, *J Am Chem Soc*, 2001, **123**, 5221-5230.
58. J. Wang, P. Cieplak and P. A. Kollman, *J Comput Chem*, 2000, **21**, 1049-1074.
59. Q. Cui, T. Sulea, J. D. Schrag, C. Munger, M. N. Hung, M. Naim, M. Cygler and E. O. Purisima, *J Mol Biol*, 2008, **379**, 787-802.
60. D. Rognan, S. L. Lauemøller, A. Holm, S. Buus and V. Tschinke, *J Med Chem*, 1999, **42**, 4650-4658.

**Table 1. Peptide-MHC stacking Interaction.** MHC binding site residues participating in stacking interactions (identified by the presence of the check mark) for (A) DQB1 alleles and (B) DRB1 alleles, with each allele complexed with MBP or EBNA1 peptide. The

predisposing alleles, both wild type (WT) or mutant (V38A, A38V, G86V, V86G) correspond to DRB1 = DRB1\*15:01, DQB1 = DQB1\*06:02, while the protective alleles correspond to DRB1 = DRB1\*16:01, DQB1 = DQB1\*05:02.

(A) DQB1 complex	MBP complexed				EBNA1 complexed			
	protective		predisposing		protective		predisposing	
MHC residues	W T	V38 A	WT	A38 V	W T	V38 A	WT	A38 V
β Phe 9			✓	✓				
β Phe 11				✓				
β Tyr 60	✓	✓						
β Arg 77		✓						
β His 81	✓	✓			✓		✓	
α Tyr 22						✓		
α His 24			✓				✓	
α Phe 26								✓
α Phe 54	✓			✓	✓		✓	✓
α Arg 61			✓	✓			✓	
α Arg 76	✓							

(B) DRB1 complex	MBP complexed				EBNA1 complexed			
	protective		predisposing		protective		predisposing	
MHC residues	W T	G86 V	WT	V86 G	W T	G86 V	W T	V86G
β Phe 26	✓	✓	✓	✓				✓
β Tyr 60		✓						
β Arg 71	✓							
β Tyr 78		✓					✓	
β His 81			✓					
α Phe 22								✓
α Phe 24								✓
α Phe 32								✓
α Phe 54	✓	✓	✓	✓				✓

**Table 2. Binding free energies of wild type haplotypes.** Binding free energies (kcal/mol) for the DQB1 and DRB1 haplotypes, in complex with MBP and EBNA1 peptides under analysis. The error reported is the standard error of the mean value of free energy obtained from MD simulation. In column 2, 4 is reported binding free energy and in column 3, 5 is reported their corresponding IC<sub>50</sub> values for alleles complexed with MBP and EBNA1 respectively. In column 6 is reported the IC<sub>50</sub> of EBNA1 complexes scaled by allele specific MBP IC<sub>50</sub>. The last column reports the difference in binding energy for each allele between the EBNA1 and the MBP peptide complex. The last two rows reports the same binding free energy difference for each peptide between predisposing and protective allele of DQB1 and DRB1 haplotypes.

	MBP		EBNA1			$\Delta G^{\text{EBNA1}} - \Delta G^{\text{MBP}}$ (kcal/mol)
	$\Delta G$ (kcal/mol)	IC <sub>50</sub> (nM)	$\Delta G$ (kcal/mol)	IC <sub>50</sub> (nM)	IC <sub>50</sub> (EBNA1)/ IC <sub>50</sub> (MBP)	
DQB1*05:02 (prot)	- 18.5±0. 6	9.1 x 10 <sup>-5</sup>	- 17.0±0. 7	1.0 x 10 <sup>-3</sup>	11	1.5±1.3
DQB1*06:02 (pred)	- 14.1±0. 8	10	- 17.5±0. 8	4.6 x 10 <sup>-4</sup>	4.6 x 10 <sup>-5</sup>	-3.4±1.6
DRB1*16:01 (prot)	- 17.5±0. 7	4.6 x 10 <sup>-4</sup>	- 12.2±0. 8	2.5	5434	5.3±1.4
DRB1*15:01 (pred)	- 16.7±0. 6	1.7 x 10 <sup>-3</sup>	- 16.0±0. 7	5.2 x 10 <sup>-3</sup>	3	0.7±1.3
$\Delta$ DQB1(*06:02 - *05:02)	4.4±1.4 kcal/mol		-0.5 ±1.5 kcal/mol			
$\Delta$ DRB1(*15:01- *16:01)	0.8±1.3 kcal/mol		-3.8±1.4 kcal/mol			

**Table 3. Binding energies of mutant haplotypes.** Binding energies (kcal/mol) upon mutation of residue 38 for the DQB1 and of residue 86 for DRB1 alleles, in complex with MBP and EBNA1 peptides under analysis. The error reported is the standard error of the mean value of free energy obtained from MD simulation. In column 2, 5 is reported binding energy and in column 3, 6 is reported their corresponding  $IC_{50}$  values for mutant alleles complexed with MBP and EBNA1 respectively. The change in binding energy upon mutation is reported in column 4 for MBP and in column 7 for EBNA1 complexes. The negative value of free energy reported in column 4 and column 7 correspond to mutation having a stabilizing effect on the pMHC complex.

	MBP			EBNA1		
	$\Delta G_{MUT}$ (kcal/mol)	$IC_{50}$ (nM)	$\Delta G_{MUT} - \Delta G_{WT}$ (kcal/mol)	$\Delta G_{MUT}$ (kcal/mol)	$IC_{50}$ (nM)	$\Delta G_{MUT} - \Delta G_{WT}$ (kcal/mol)
V38A (prot)- DQB1*05:0 2	-18.3±0.6	$1.3 \times 10^{-4}$	0.2±1.2	-17.9±0.6	$2 \times 10^{-4}$	-0.9±1.3
A38V (pred)- DQB1*06:0 2	-15.6±0.7	$10 \times 10^{-3}$	-1.5±1.5	-18.3±0.8	$1.3 \times 10^{-4}$	-0.8±1.6
G86V (prot)- DRB1*16:01	-18.0±0.6	$2 \times 10^{-4}$	-0.5±1.3	-13.0±0.8	0.7	-0.8±1.5
V86G (pred)- DRB1*15:01	-16.0±0.7	$5.2 \times 10^{-3}$	0.7±1.5	-18.4±0.8	$1.1 \times 10^{-4}$	-2.4±1.5

### Figure legends

**Fig. 1. Haplotype phylogenetic classification.** DRB1-DQB1 haplotypes represent evidence and protective haplotypes for Sardinian population are boxed, the others are predisposing.

**Fig. 2. HLA-DQ protein in complex with MBP peptide inserted in water box.** Chains A (left, blue) and B (right, red) are shown in cartoon representation, MBP peptide (center) is shown as ball and stick, and water molecules (surrounding) are represented as red spheres. The MHC binding cleft is boxed by black dashed lines.

**Fig. 3. The four compartments of MHC binding cleft.** (A) For HLA DQB1 protein: D1 ( $\alpha$ 1 53-54,  $\beta$ 1 84-85) in red; D2 ( $\alpha$ 1 57-59,  $\beta$ 1 77-82) in blue; D3 ( $\alpha$ 1 64-69,  $\beta$ 1 67-72) in green and D4 ( $\alpha$ 1 72-77,  $\beta$ 1 56-61) in yellow, and  $\beta$ 1:38 is position in DQB1 chain where the residue has been mutated. (B) For HLA DRB1 protein : D1 ( $\alpha$ 1 50-51,  $\beta$ 1 85-86) in red; D2 ( $\alpha$ 1 53-55,  $\beta$ 1 78-83) in blue; D3 ( $\alpha$ 1 60-65,  $\beta$ 1 65-70) in green and D4 ( $\alpha$ 1 68-73,  $\beta$ 1 56-61) in yellow, and  $\beta$ 1:86 is position in DRB1 chain where residue has been mutated. The MHC residues are shown in surface representation. The pockets P1, P4, P7, and P9 are shown as colored squares.

**Fig. 4. Binding cleft width distribution of DQB1 alleles.** (A) and (B) report the width distribution of region D1 and D4, respectively, for DQB1\*05:02 wild type or mutant (V38A) allele, for the free and bound peptide MHC systems. In inset of (A), the width distribution for protective DQB1 wild type and mutant V38A in complex with MBP in region D1, while in inset of (B) in region D4 are shown. (C) and (D) report the width distribution of region D2 and D3, respectively, for DQB1\*06:02 wild type or mutant (A38V) allele, for the free and bound peptide MHC systems. In inset of (C), the width distribution for predisposing DQB1 wild type and mutant A38V in complex with EBNA1 in region D2 is shown. In inset of (D),

the width distribution for predisposing DQB1 wild type and mutant A38V in complex MBP in region D3 is reported.

**Fig. 5. Binding cleft width distribution of DRB1 alleles.** (A) and (B) report the width distribution of the four regions for protective DRB1 (DRB1\*16:01), for wild type or mutant (G86V) allele pMHC complexes. (C) and (D) report the width distribution of the four regions for predisposing DRB1 (DRB1\*15:01), for the wild type and mutant (V86G) allele pMHC complexes.

**Fig. 6. H-bond interaction network for peptide-DQB1 complexes.** Peptide residues participating in H-bond interactions are shown as spheres (magenta) and MHC residues are shown in ball and stick (magenta) representation. The names of functional groups of the residues involved are abbreviated in some cases as follows: phenol (Ph), imidazole (Imd), amine (-NH<sub>2</sub>), carboxylic acid (-COOH) and alcohol (-OH). To distinguish between the main and side-chain functional groups of the residues “\*” symbol is used. (A) MBP-DQB1\*05:02 complex (protective MHC allele). (B) MBP-DQB1\*06:02 complex (predisposing MHC allele). (C) EBNA1- DQB1\*05:02 complex (protective MHC allele). (D) EBNA1-DQB1\*06:02 complex (predisposing MHC allele). The whole binding groove is shown in cartoon representation (grey), the mutation region (DQB1 38) is shown in surf (yellow) representation, and peptides are shown in tube representation (MBP peptide in black and EBNA1 peptide in red).

**Fig. 7.** H-bond interaction network for the DQB1 wild type and mutant alleles in complex with MBP peptide. For details regarding the names of functional groups, see legend in Fig. 6.

**Fig. 8.** H-bond interaction network for the DQB1 wild type and mutant alleles in complex with EBNA1 peptide. For details regarding the names of functional groups, see legend in Fig. 6.

**Fig. 9.** H-bond interaction network for the DRB1 wild type and mutant alleles in complex with MBP peptide. For details regarding the names of functional groups, see legend in Fig. 6.

**Fig. 10.** H-bond interaction network for the DRB1 wild type and mutant alleles in complex with EBNA1 peptide. For details regarding the names of functional groups, see legend in Fig. 6.

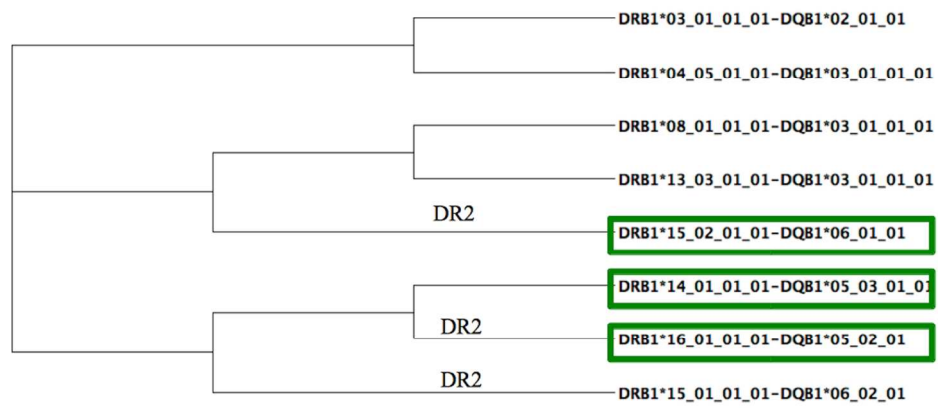


Fig. 1. Haplotype phylogenetic classification. DRB1-DQB1 haplotypes represent evidence and protective haplotypes for Sardinian population are boxed, the others are predisposing.  
75x32mm (600 x 600 DPI)

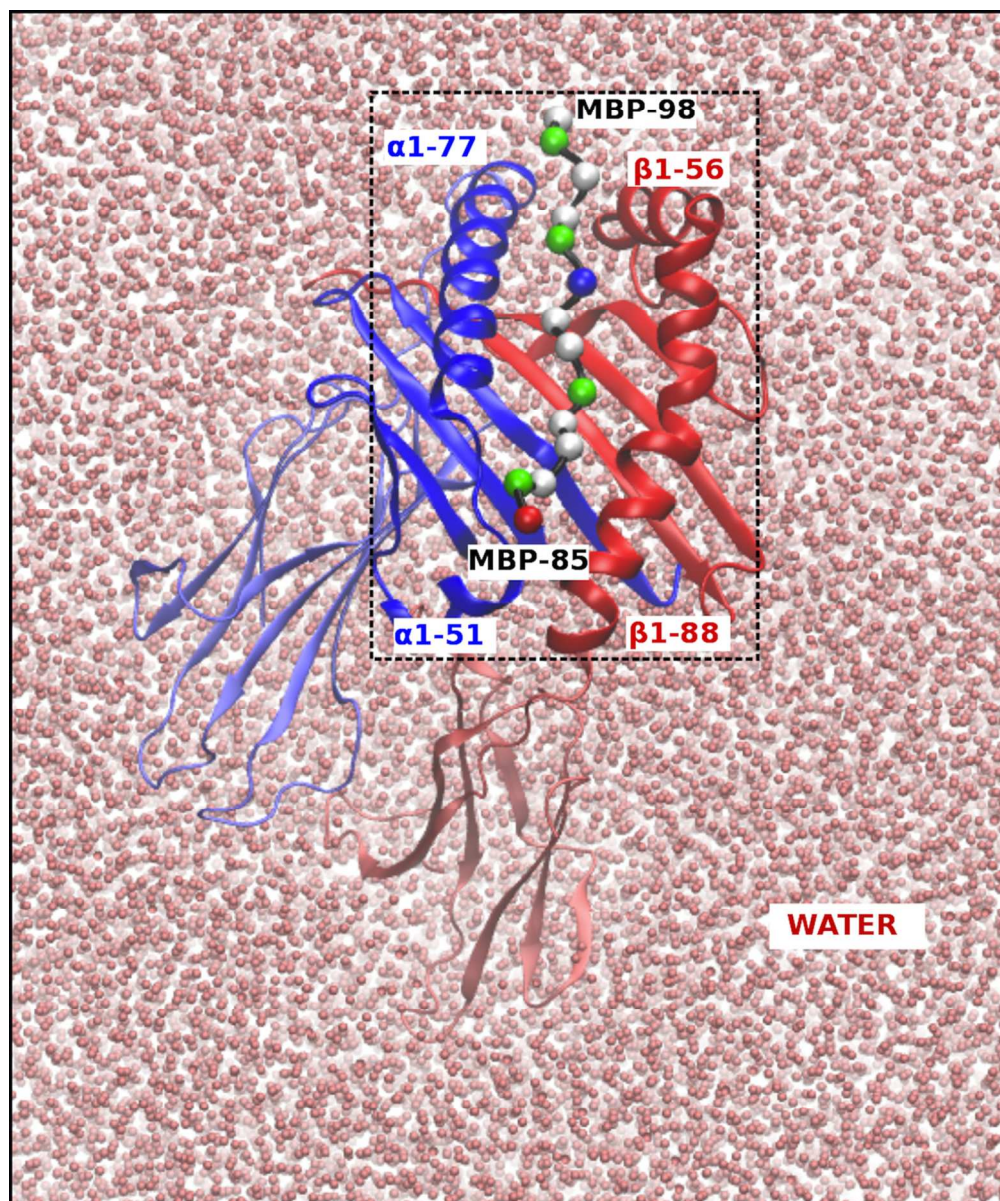


Fig. 2. HLA-DQ protein in complex with MBP peptide inserted in water box. Chains A (left, blue) and B (right, red) are shown in cartoon representation, MBP peptide (center) is shown as ball and stick, and water molecules (surrounding) are represented as red spheres. The MHC binding cleft is boxed by black dashed lines.

119x142mm (300 x 300 DPI)

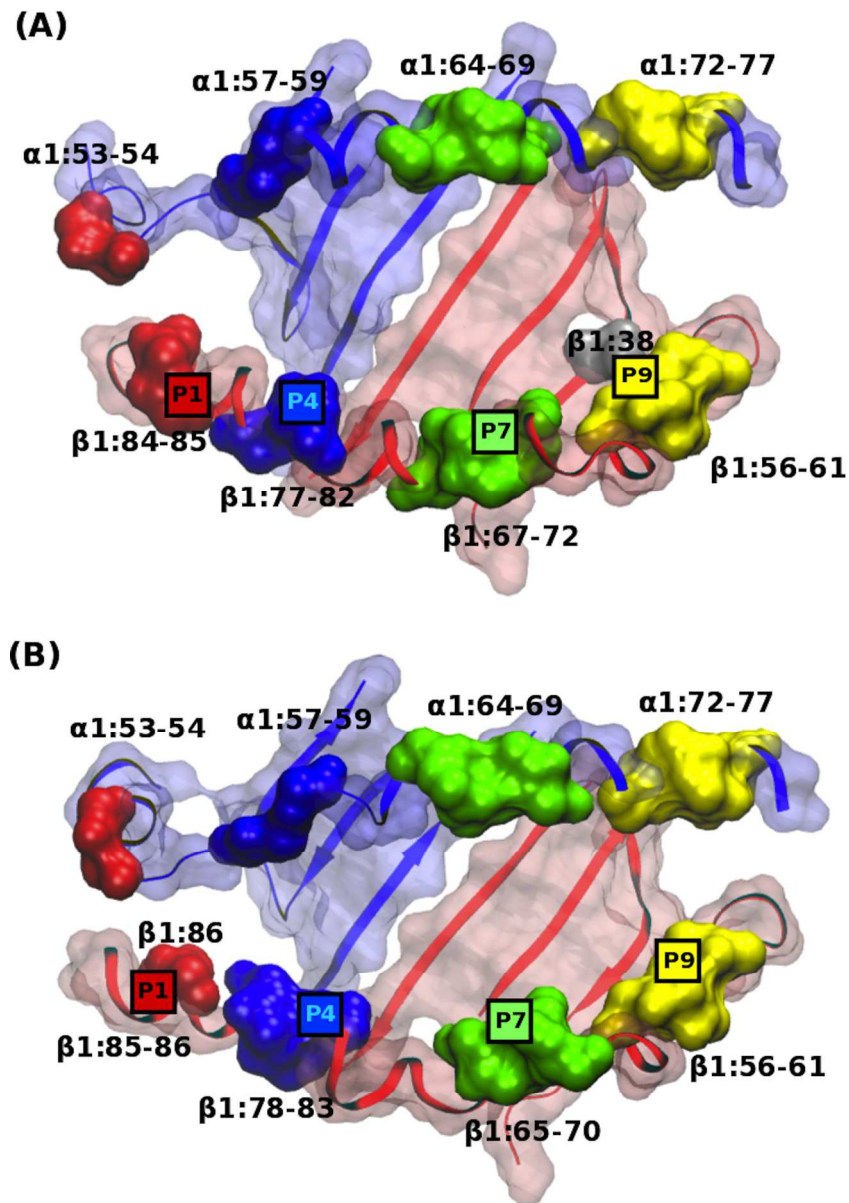


Fig. 3. The four compartments of MHC binding cleft. (A) For HLA- DQ protein: D1 ( $\alpha 1$  53-54,  $\beta 1$  84-85) in red; D2 ( $\alpha 1$  57-59,  $\beta 1$  77-82) in blue; D3 ( $\alpha 1$  64-69,  $\beta 1$  67-72) in green and D4 ( $\alpha 1$  72-77,  $\beta 1$  56-61) in yellow, and  $\beta 1:38$  is position in DQB1 chain where the residue has been mutated. (B) For HLA- DRB1 protein : D1 ( $\alpha 1$  50-51,  $\beta 1$  85-86) in red; D2 ( $\alpha 1$  53-55,  $\beta 1$  78-83) in blue; D3 ( $\alpha 1$  60-65,  $\beta 1$  65-70) in green and D4 ( $\alpha 1$  68-73,  $\beta 1$  56-61) in yellow, and  $\beta 1:86$  is position in DRB1 chain where residue has been mutated. The MHC residues are shown in surface representation. The pockets P1, P4, P7, and P9 are shown as colored squares.

143x206mm (600 x 600 DPI)

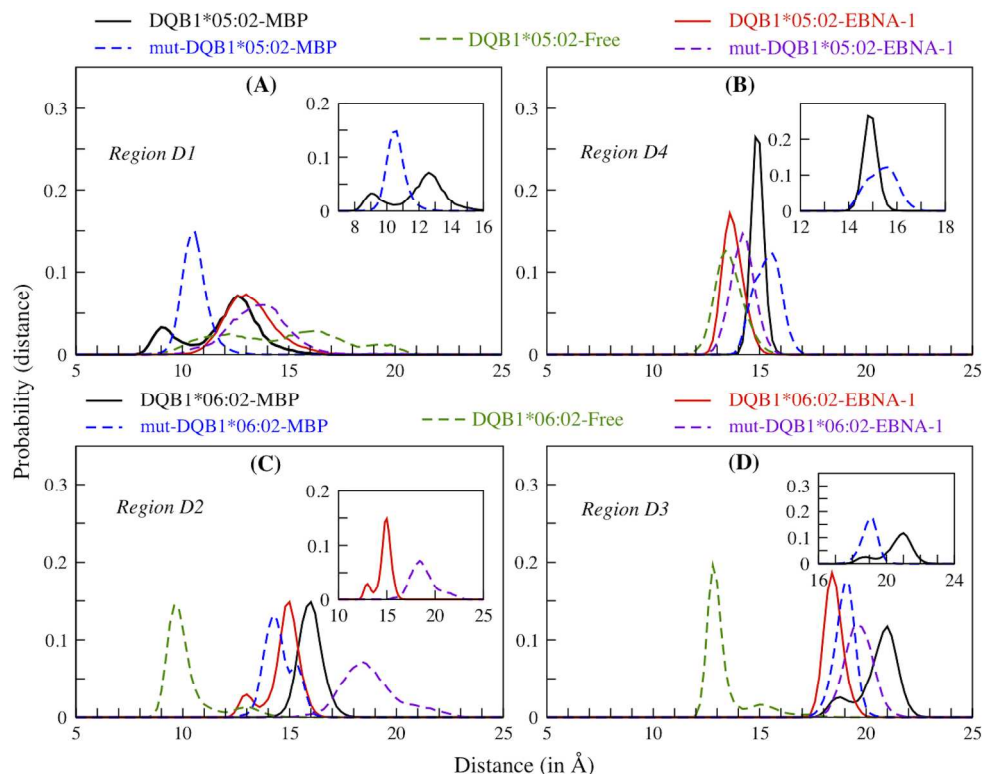


Fig. 4. Binding cleft width distribution of DQB1 alleles. (A) and (B) report the width distribution of region D1 and D4, respectively, for DQB1\*05:02 wild type or mutant (V38A) allele, for the free and bound peptide MHC systems. In inset of (A), the width distribution for protective DQB1 wild type and mutant V38A in complex with MBP in region D1, while in inset of (B) in region D4 are shown. (C) and (D) report the width distribution of region D2 and D3, respectively, for DQB1\*06:02 wild type or mutant (A38V) allele, for the free and bound peptide MHC systems. In inset of (C), the width distribution for predisposing DQB1 wild type and mutant A38V in complex with EBNA1 in region D2 is shown. In inset of (D), the width distribution for predisposing DQB1 wild type and mutant A38V in complex MBP in region D3 is reported.

131x101mm (600 x 600 DPI)

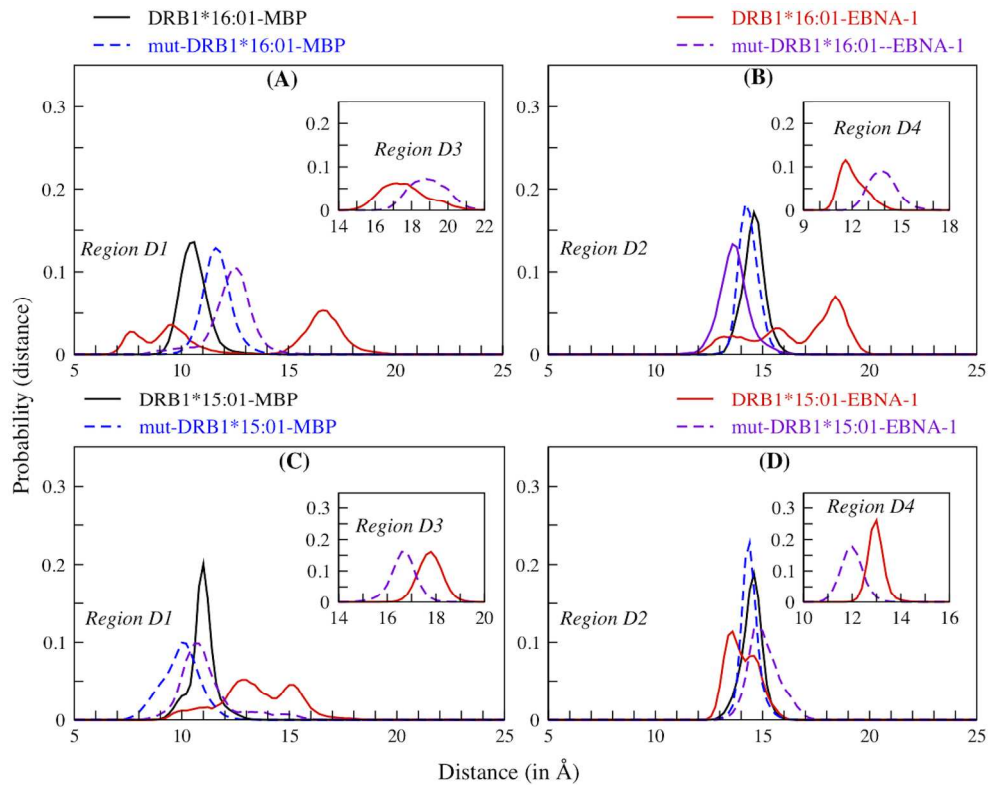


Fig. 5. Binding cleft width distribution of DRB1 alleles. (A) and (B) report the width distribution of the four regions for protective DRB1 (DRB1\*16:01), for wild type or mutant (G86V) allele pMHC complexes. (C) and (D) report the width distribution of the four regions for predisposing DRB1 (DRB1\*15:01), for the wild type and mutant (V86G) allele pMHC complexes.

133x105mm (600 x 600 DPI)

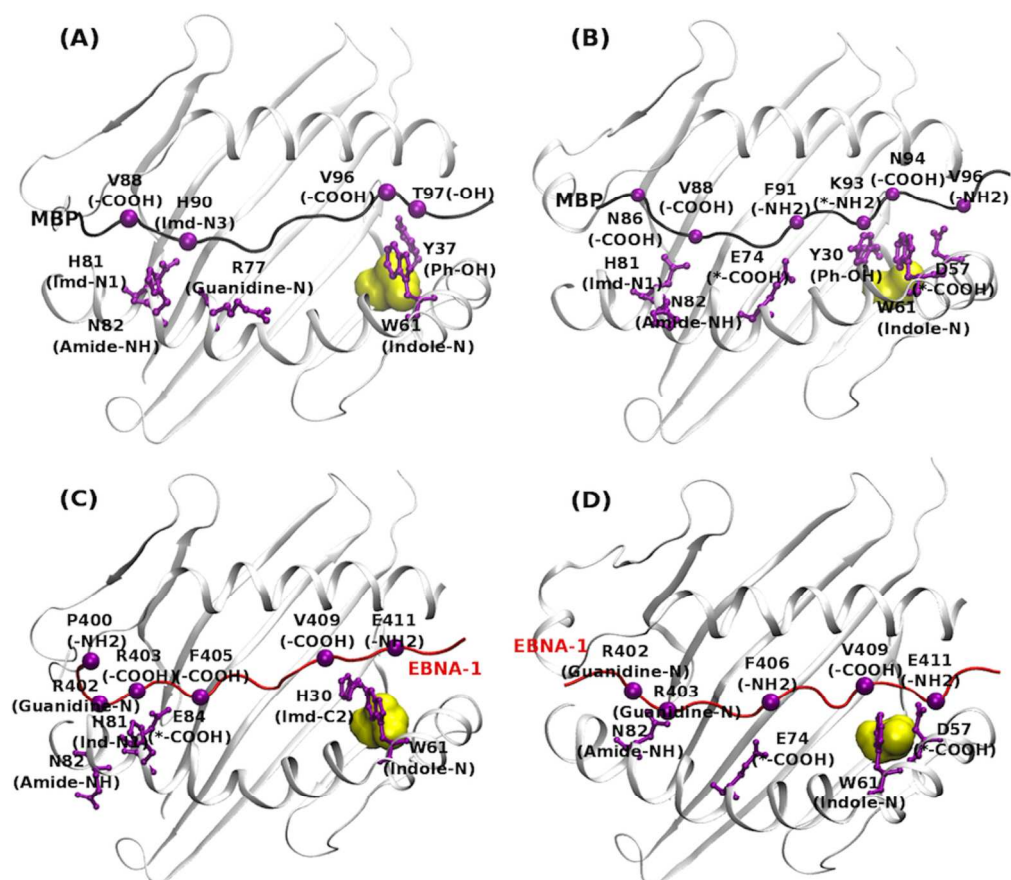


Fig. 6. H-bond interaction network for peptide-DQB1 complexes. Peptide residues participating in H-bond interactions are shown as spheres (magenta) and MHC residues are shown in ball and stick (magenta) representation. The names of functional groups of the residues involved are abbreviated in some cases as follows: phenol (Ph), imidazole (Imd), amine (-NH<sub>2</sub>), carboxylic acid (-COOH) and alcohol (-OH). To distinguish between the main and side-chain functional groups of the residues "\*" symbol is used. (A) MBP-DQB1\*05:02 complex (protective MHC allele). (B) MBP-DQB1\*06:02 complex (predisposing MHC allele). (C) EBNA1-DQB1\*05:02 complex (protective MHC allele). (D) EBNA1-DQB1\*06:02 complex (predisposing MHC allele). The whole binding groove is shown in cartoon representation (grey), the mutation region (DQB1 38) is shown in surf (yellow) representation, and peptides are shown in tube representation (MBP peptide in black and EBNA1 peptide in red).

143x129mm (300 x 300 DPI)

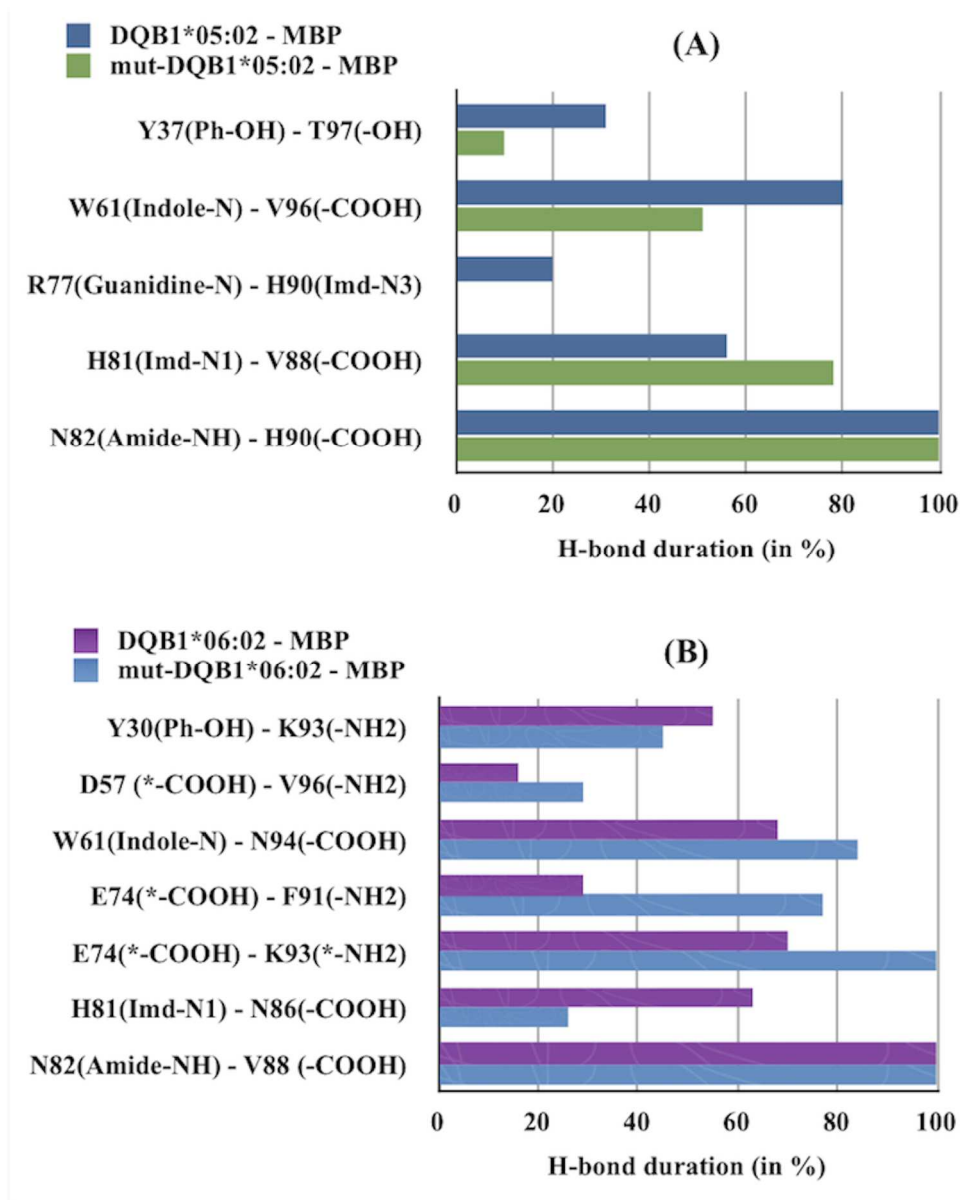


Fig. 7. H-bond interaction network for the DQB1 wild type and mutant alleles in complex with MBP peptide. For details regarding the names of functional groups, see legend in Fig. 6.  
 148x184mm (300 x 300 DPI)

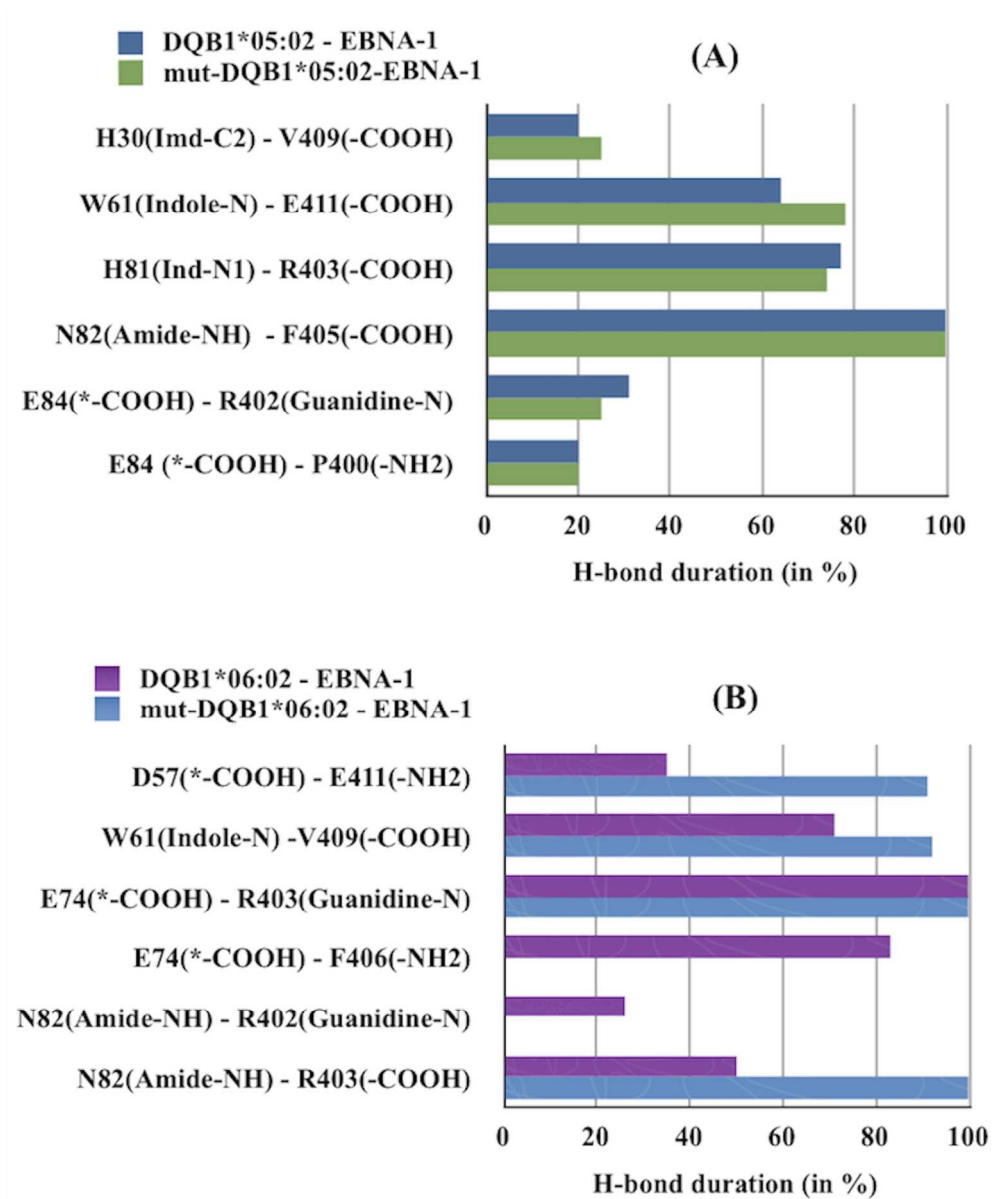


Fig. 8. H-bond interaction network for the DQB1 wild type and mutant alleles in complex with EBNA1 peptide. For details regarding the names of functional groups, see legend in Fig. 6.  
143x170mm (300 x 300 DPI)

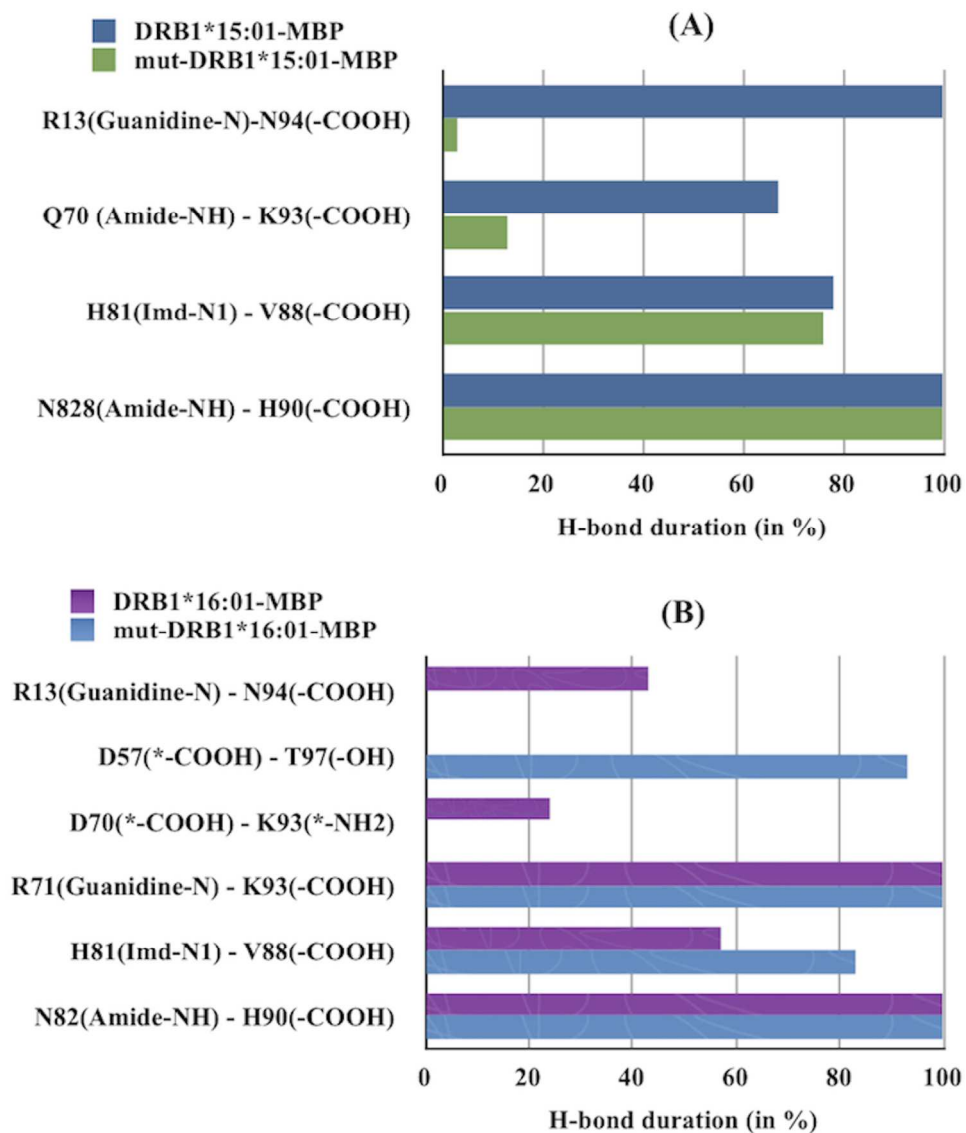


Fig. 9. H-bond interaction network for the DRB1 wild type and mutant alleles in complex with MBP peptide. For details regarding the names of functional groups, see legend in Fig. 6.  
138x159mm (300 x 300 DPI)

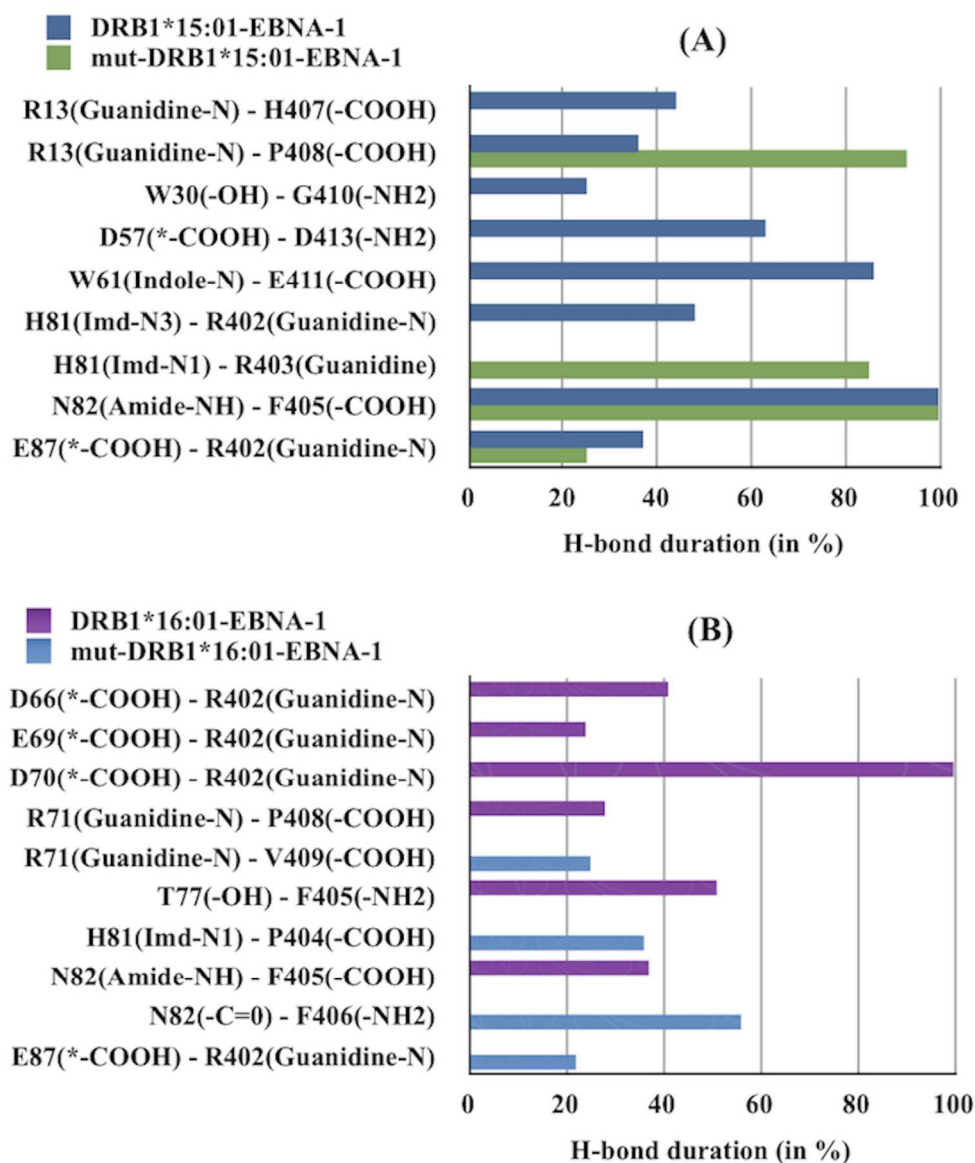


Fig. 10. H-bond interaction network for the DRB1 wild type and mutant alleles in complex with EBNA1 peptide. For details regarding the names of functional groups, see legend in Fig. 6.  
142x169mm (300 x 300 DPI)